High-Power HTS Microstrip Filters for Wireless Communication

Guo-Chun Liang, *Senior Member, IEEE*, Dawei Zhang, *Member, IEEE*, Chien-Fu Shih, Marie E. Johansson, Richard S. Withers, *Member, IEEE*, Daniel E. Oates, A. C. Anderson, P. Polakos, P. Mankiewich, E. de Obaldia, and R. E. Miller

Abstract— **The performance of narrowband microstrip filters with low insertion loss and high power-handling capabilities made from $YBa_2Cu_3O_{7-\delta}$ (YBCO) high-temperature superconducting (HTS) thin films is presented. Results are shown for two different designs that were chosen to optimize the power-handling capability. Both filters have a 2-GHz center frequency and 5 poles that incorporate coupled resonators with 10-Ω internal impedances. They were made on 5-cm-diameter $LaAlO_3$ substrates. Both designs use parallel-coupled feed lines to avoid current crowding. The first design includes backward- and forward-coupled filters, has 1% bandwidth, and has handled over 25 watts of input power at 10 K with less than 0.25 dB compression. The second design has 1.2% bandwidth and uses only forward-coupled resonators. The dissipation loss is less than 0.2 dB at 45 K and it has a third-order intercept of 62 dBm. Another similar filter handled 36 watts of power at 45 K with less than 0.15 dB compression across the passband. We have developed a technique to visualize the power dissipation of the filter by observing the bubbles created by the filter when submerged in liquid helium, showing areas with local defects or where the current distribution is at its peak value. We also discuss several planar high-power filter issues, including material selection and fabrication, device configuration trade-offs, filter structure optimization, and design approaches to maximize power-handling capacity.**

I. Introduction

THE EXPLOSION IN THE DEMAND for wireless communications stresses the capabilities of current cellular systems [1]–[3]. In order to enhance system performance, filters with sharp skirts, low insertion loss, and high power-handling capability are critical.

In one popular type of cellular base station, signals in different voice channels are first combined at relatively low power levels and then amplified to the required power level (e.g., 250 W). While this system allows flexibility in operating frequencies, bandwidths, and the number of combined channels, it imposes stringent demands on the linearity of the power amplifier. The linearity of the amplifier can be increased with feed-forward or pre-distortion techniques, but these techniques can be very complex and expensive. A more practical, and probably more cost-effective, approach is to use an amplifier with some low level of intermodulation distortion within the transmission band. This would, however, violate the FCC intermodulation regulations outside the operator's frequency band and, more important to the operator, it may reduce the linear and/or spur-free dynamic range of the base-station receiver. A common solution is to use a clean-up filter such as a waveguide, an air-dielectric, or a comb-line filter, after the amplifier. A superconducting clean-up filter could be used to greatly reduce the insertion loss and, by using a filter with a larger number of poles, increase the out-of-band rejection, but it must be able to handle tens or hundreds of watts. In particular, the intermodulation produced by the nonlinearity of the high-temperature superconductor filter itself should be well within the acceptable limits of the system.

Compact planar filters using HTS thin films have been shown to provide insertion loss and out-of-band rejection superior to those made by conventional technologies [4]–[8]. Filters made with thin-film technology have been limited, until recently, to operating power levels in the tens of milliwatts [6], [9]. Such filters have been made in several configurations including microstrip line, stripline and coplanar waveguide (CPW). Stripline resonators have higher unloaded Q's for a given film surface resistance and no radiation losses, but they are difficult to assemble. Additionally, the center frequency of a narrowband filter may not be stable because of microphonics. CPW structures eliminate the requirement of double-sided wafers and are easy to fabricate and assemble. Unfortunately, the insertion loss is often larger than allowable for potential applications. Furthermore, the air bridges sometimes required to keep the ground planes at equal potential, complicate the implementation of the filter. Microstrip circuits, although having higher radiation losses than stripline circuits, are very simple to make and package.

We have chosen a microstrip structure for our filters for the recently FCC-allocated 2 GHz wireless frequency band. In the design of the filters, we placed emphasis on increasing the power-handling capabilities by widening the lines and reducing the peak current density. We used 5-cm-diameter, 0.5-mm-thick $LaAlO_3$ which has a low dielectric loss ($\tan\delta \sim 3\times10^{-5}$) and a relative dielectric constant of about 24. Fig. 1 is a photograph of one 5-pole interdigital filter. It has 0.7% fractional bandwidth centered at 2 GHz [10].

Microwave filters have been designed and made on both stripline and microstrip line structures based on a backward coupling phenomenon, which uses overlapped

Manuscript received March 10, 1995; revised July 10, 1995. This work was supported in part by ARPA under the auspices of the Consortium for Superconducting Electronics (CSE).

G.-C. Liang, D. Zhang, C.-F. Shih, M. E. Johansson, R. S. Withers are with Conductus, Inc., Sunnyvale, CA 94086 USA.

D. E. Oates, A. C. Anderson are with Lincoln Laboratory, Massachusetts Institute of Technology, Lexington, MA 02173-9108 USA.

P. Polakos, P. Mankiewich, E. de Obaldia and R. E. Miller are with AT&T and Bell Laboratories, Murray Hill, NJ 07974 USA.

IEEE Log Number 9415450.

quarter-wavelength parallel lines. The backward coupling of the parallel-coupled lines reaches its maximum coupling when the lines are quarter-wave overlapped, and reaches its minimum when they are half-wave overlapped. The strength of this backward coupling changes periodically with a period of a half wavelength. As is well known, it is a challenge to make filters with very narrow bandwidths because the required weak coupling implies widely spaced resonators. The forward coupling caused by the even- and odd-mode velocity difference has to be considered, since the required coupling of the adjacent lines must be weaker than 40 dB for a typical 5-pole, 1% bandwidth filter. However, narrow-band filters can be built based purely on the forward-coupling structure. Although a similar structure has been reported [5], we offer a more complete analysis of the forward-coupled structure [10]–[12]. A narrowband (1.2%) forward-coupled filter at 2 GHz is presented. By eliminating the backward coupling, we can arrange the elements close together, making a compact filter and still maintaining the weak coupling necessary for narrowband operation.

II. Filter Design

A. Simulation Approach and Filter Structures

In the filter design, we combine both analytical and numerical methods. The filter is synthesized based on its low-pass prototype. After the synthesis of the filter based on the empirical formulas and/or analytical expressions, we analyzed the filter using an electromagnetic simulator and then iterated the design, if necessary.

There are several types of numerical tools for filter analysis. One is circuit-model-based simulation. This type of simulation relies on the use of analytical formulas and has only a limited component library and parameter range (e.g., most cannot handle a $LaAlO_3$ substrate because of its high dielectric constant and cannot handle very narrowband filter designs because of ultra-weak coupling coefficients and nonadjacent coupling issues). These tools are sometimes limited to single-layer circuits and ignore parasitic coupling and radiation. Another type of simulation tool is a field-based simulation, including true 3-dimensional finite-element, finite-difference, and integral-equation-based simulation. Finite-difference and finite-element approaches can solve very general problems, but they require large amounts of memory and computer time. We are using an integral-equation approach based on full-wave analysis. It can simulate radiation, dispersion, and arbitrary geometric coupling and can handle materials with complex dielectric constants or complex surface impedances [13]. In the simulation, the superconductor has been specified either by complex surface impedance, or simply as a conductor with very high conductivity. Comparisons of the different treatments have been reported for transmission lines and antennas [14]–[16].

B. Discussion of Power-Handling Capability

In this section, we present the design approach to enhance the power-handling capability of the planar filter for a given material. The nonlinear effects of the superconducting material occur when the RF current density (or the RF magnetic field) exceeds some threshold value [17]–[20]. We use a linear model valid below this threshold to simplify the analysis.

The sheet current at any point in the filter will scale as the square root of the input power. We need to minimize the constant of proportionality between the peak sheet current density and the input power. This is a great challenge in designing quasiplanar circuits, because of the tendency for current densities to have a maximum at the edges of the planar transmission lines [20].

There are several possible ways in which we can minimize the peak sheet current density: 1) reduce the nonuniformity of current across the filter cross section, as expressed by the ratio $\beta = K_{\max}/K_{\text{av}}$, where $K_{\max}$ is the peak sheet current density and K_{av} is the sheet current density averaged across the device cross section; 2) increase the linewidth so that there is more conductor available for carrying current; 3) increase the amount of power carried in a given transmission line for a given current, i.e., increase the line's characteristic impedance by using a thicker dielectric or lower effective dielectric constant (n.b.: but *not* a narrower line); and 4) decrease the Q-multiplication factor of the filter.

It is useful to look at the interplay of these factors in a simple context. First of all, assume a lossless filter. This is reasonable, since with insertion loss of less than 0.5 dB, much more power is flowing through the filter than is being dissipated within it. Now assume that the resonators within the filter are designed to have a certain loaded quality factor Q_L, which scales as the reciprocal of the fractional bandwidth desired. We know that the peak energy stored within a resonator, E_{res}, is $Q_L/2\pi$ times twice the energy which flows through the filter during one cycle, or

$$E_{\text{res}} = \frac{Q_L P_{\text{in}}}{\pi f} \tag{1}$$

where P_{in} is the input power and f is the operating frequency. Since $P_{\text{res}} = fE_{\text{res}}/n$, where P_{res} is the instantaneous power flow in one direction within the resonator and n is the length of the resonator expressed in half-wavelengths (i.e., the overmode factor), the peak current at standing wave peaks along the length of the resonator is

$$I_{\text{peak}} = \sqrt{\frac{8P_{\text{res}}}{Z_0}} = \sqrt{\frac{8fE_{\text{res}}}{nZ_0}} = \sqrt{\frac{8Q_L P_{\text{in}}}{\pi n Z_0}} \tag{2}$$

where Z_0 is the characteristic impedance of the resonator. The peak current I_{peak} will change very little if we take the insertion loss into consideration.

For simplicity, assume that we have a microstrip resonator of width w and dielectric thickness d, with $w \gg d$. Then $Z_0 = \sqrt{\frac{\mu_o}{\varepsilon_{\text{eff}}}}\frac{d}{w} = \eta\frac{d}{w}$, where ε_{eff} is the effective substrate dielectric constant. We then have

$$I_{\text{peak}} = \sqrt{\frac{4wQ_L P_{\text{in}}}{\pi n \eta d}}. \tag{3}$$

The peak cross-sectional-average sheet current density is then

$$(K_{\mathrm{av}})_{\mathrm{peak}} = \frac{I_{\mathrm{peak}}}{w} = \sqrt{\frac{4Q_L P_{\mathrm{in}}}{\pi n \eta w d}}. \tag{4}$$

This is easily inverted to express the input power at the onset of nonlinearities, P_{NL}, as a function of the current-carrying capacity of the material expressed as the sheet current density at the onset of nonlinearities, K_{NL}

$$P_{\mathrm{NL}} = \frac{\pi n \eta d w}{4Q_L}\left(\frac{K_{\mathrm{NL}}}{\beta}\right)^2 \tag{5}$$

where $\beta = K_{\max}/K_{\mathrm{av}}$ is the previously defined cross-sectional nonuniformity factor. Thus, it is readily seen that it is advantageous to design for *wide* lines on *thick* dielectrics with *low* effective dielectric constants.[1] Furthermore, it is helpful to design not with half-wave resonators but with overmoded resonators ($n > 1$).

The above discussion is a simplified case. The discussion can be made more general [21]. For a given filter, assuming no reflection loss at the center frequency ω_0, the pulse power which can be transmitted through an n-pole bandpass filter at onset of voltage or current breakdown in the kth resonator at the center frequency is linearly proportional to the fractional bandwith, an overmode factor (length of the resonator measured in half-wavelengths), and the pulse-power capacity of a transmission line with an identical cross-section to that of the filter's resonators. It is inversely proportional to the corresponding element in the equivalent low-pass prototype circuit g_k. Because the g_k's are usually not the same for each element in the low-pass prototype, the pulse-power capacity of the overall filter is limited by the resonator element with the largest values of g_k. It is possible to maximize the filter power-handling capability by adjusting the g_k values while still keeping the desired frequency response.

However, the above-stated relationship of resonator power and g factors only applies at the center frequency. To examine the current distribution at other frequencies and the resulting frequency dependence of the power-handling capability, we begin with the lumped-element equivalent circuit of the filter shown in Fig. 1. Each resonator (10-Ω half-wavelength resonators) is represented by an RLC tank circuit, and these resonators are coupled together with coupling capacitors C_{ci} as shown in Fig. 2(a).

We simulate the circuit using SPICE. Fig. 2(b) and (c) show the cross-sectional average of the rms current density (I_{peak} divided by cross-sectional area) midway along the length of each resonator, where the current is at its maximum, as a function of frequency. These data were obtained at an input power of 0 dBm. It should be pointed out that this current density is the average value over the resonator cross section midway along the length of each resonator, not the peak current at the microstrip edge [22]. Resonator 1 is close to the source. Note that the current density distribution among different resonators is not symmetrical about the center of the filter. The second resonator from the input has the highest current, and thus it limits the overall power-handling capability of the filter. For all resonators except the last, the highest current density occurs at the band edges, which results in considerably lower power-handling capability.

[1] This could be implemented by, for example, using suspended stripline.

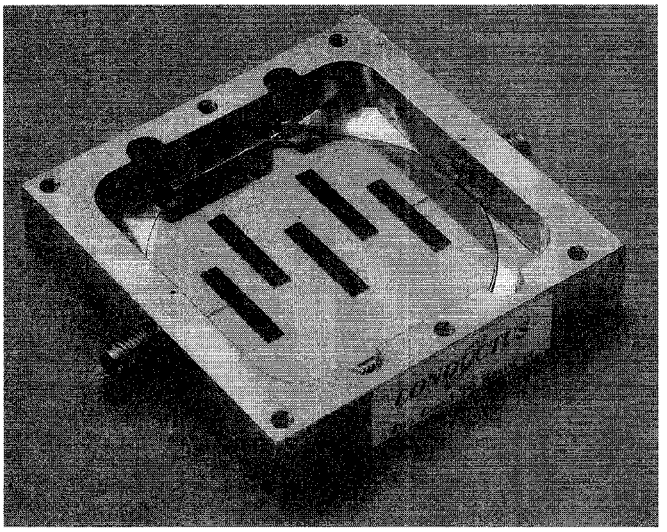

Fig. 1. A 5-pole microstrip interdigital filter designed for 0.7% bandwidth at 2 GHz [10]. The resonators have 10-Ω characteristic impedance. The input and output feed line impedances are both 50 Ω.

Several high-power YBCO filters on 2 inch $LaAlO_3$ substrates have been reported [10], [23], and [24]. As mentioned, Fig. 1 is the layout of one of the filters in [10] which has a 0.7% fractional bandwidth. This filter was made with a laser-ablated double-sided YBCO film on a $LaAlO_3$ substrate. In this work, however, the input and output feed lines are directly tapped to the first and last resonators. This feed configuration limits the power the filter can handle due to the current crowding at the feed line and first resonator junctions. Fig. 3 depicts a simulation of the vector current density at one instant in the vicinity of the tap line of the filter in Fig. 1. The simulation was performed using IE3D, a full-wave simulation package. The current crowding point is clearly shown in Fig. 3. Both the length and the width of the arrows are proportional to the current density. As expected, the current is crowded at the edge of the resonator. Feed lines using this tapping configuration are easy to design and agree well with the experiment at low input power, but consistently fail at the tap point when sufficient power is applied to the filter. While the third-order intercept of this filter is 39 dBm at 77 K and 64 dBm at 56 K, the real input power is limited probably by thermal dissipation. Besides the limitation of the power handling capability, the filter response also has a dip at near upper band due to nonneighboring coupling. In this work, we made two new designs which alleviate these problems; 1) mixed backward- and forward-coupled filter and 2) purely forward-coupled filter.

C. Backward- and Forward-Coupled Filter Design

The first filter design combines forward- and backward-coupled resonators. As we know for two coupled microstrip lines, backward coupling is maximized when two coupled resonators have a one-quarter wavelength overlap and is minimized when two half-wavelength resonators are fully

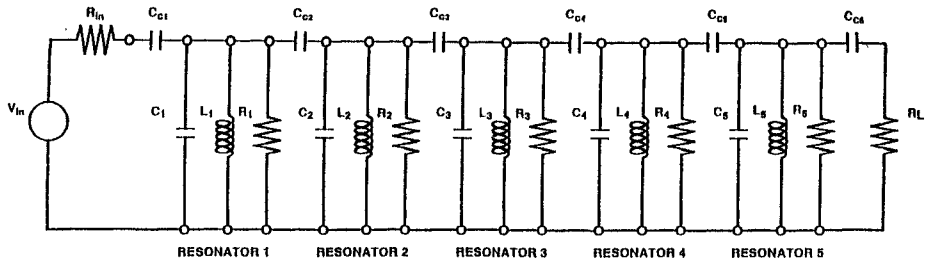

C_1=12.129 pF
C_2=12.416 pF
C_3=12.432 pF
C_4=12.416 pF
C_5=12.129 pF

C_{c1}=C_{c6}=0.358 pF
C_{c2}=C_{c5}=0.007 pF
C_{c3}=C_{c4}=0.005 pF

L_1=L_2=L_3=L_4=L_5=0.505 nH

R_1=R_2=R_3=R_4=R_5=6 35 Q_0 Ω

(a)

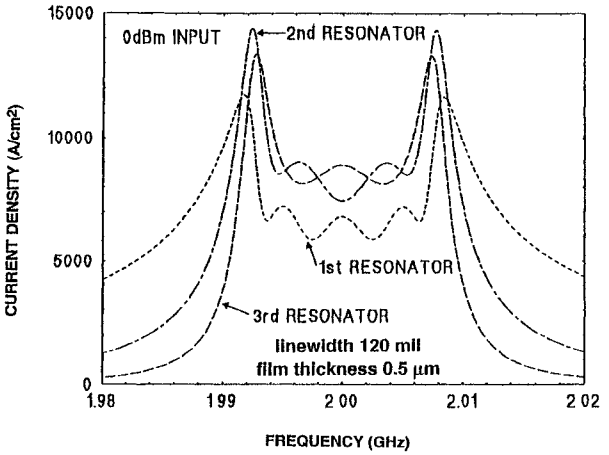

(b)

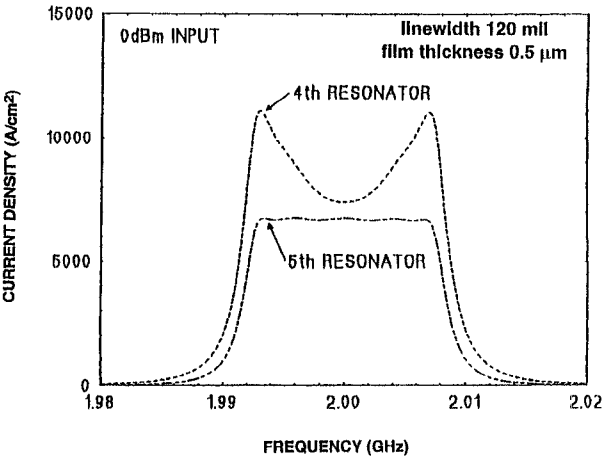

(c)

Fig. 2. (a) Lumped-element model of filter in Fig. 1. Q_0 is the unloaded quality factor of the resonators and is assumed to be 50,000 in the model. Each half-wavelength resonator is represented by a R-L-C tank circuit. The circuit parameters are so chosen that the microstrip resonator and lumped-element resonator have the same frequency responses. (b) The simulated cross-sectional average of the rms current density midway along the length of each resonator where the current is at its maximum. The simulation is done with 0-dBm input power. The film thickness is assumed to be 4000 Å. Resonator 1 is close to the source and resonator 3 is in the middle. (c) The simulated cross-sectional average of the rms current density midway along the length of each resonator under the same conditions as Fig. 2(b). Resonator 5 is close to the load.

aligned. Forward coupling, on the other hand, results from an even- and odd-mode phase velocity difference and plays a dominant role when two half-wavelength resonators are fully aligned, because the backward-coupling is then minimized. By the combination of resonators with different dominant coupling, we achieve filters with narrow bandwidth and high power-handling capability. Fig. 4 shows the backward- and forward-coupled filter.

In contrast to the tapped feed line of Fig. 1, the filter shown in Fig. 4 uses a parallel-coupled feed line. Parallel coupled feed line increases the filter's power handling capability for three reasons. First, parallel coupling reduce the peak current distribution on the edge of the resonators, thus eliminating the current crowding spot present in tapped input configurations. Second, in the parallel-coupled configuration, as the input power increases, the surface resistance of the feed line increases. As a result, the matching condition between the feed line and the first resonator is no longer met, which limits the amount of input power to the filter. Third, a thick layer of a normal metal may be deposited on the top of the YBCO film feed line to permit the feed lines to carry a higher input power without an increase in insertion loss. At low power, the superconducting feed line carries the current with a very small loss. As the power increases, the surface resistance of the superconductor increases, and the normal metal carries more of the power, thus avoiding the breakdown of the superconducting feed line that occurs with tapped feed lines.

As shown in Fig. 4, the three center resonators are coupled together dominantly by forward coupling, while the first and last resonators are coupled mainly by backward coupling. This arrangement eliminates the nonadjacent coupling present in the filter reported earlier (see Fig. 1 in [10]). The input and output feed lines are parallel-coupled into the outermost resonators, eliminating the current crowding at the junction of the feed lines and those resonators.

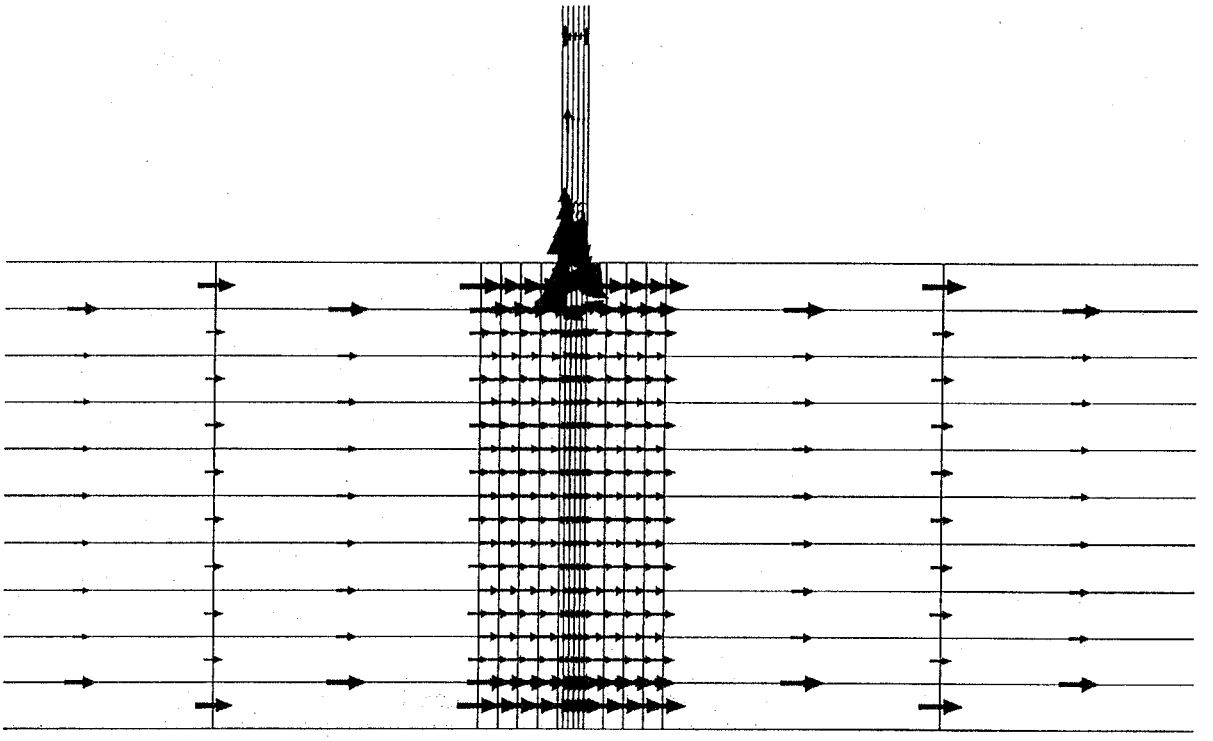

Fig. 3. The vector plot of the predicted current density on the first resonator of the 10-Ω microstrip filter of Fig. 1. Both length and width of the arrow are proportional to the current density.

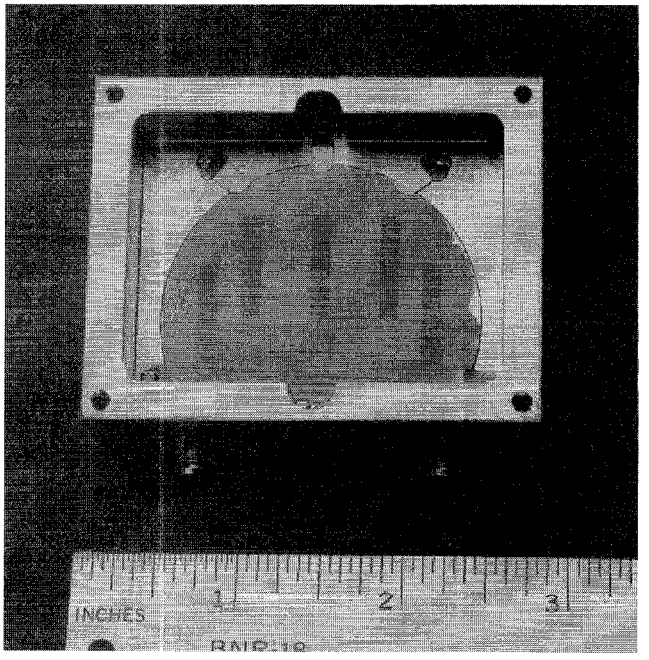

Fig. 4. A forward- and backward-coupled filter at 2 GHz. The filter has 1.2% bandwidth and 10-Ω characteristic impedance. The three resonators in the center are almost aligned.

D. Forward-Coupled Filter Design

As mentioned in the introduction, forward-coupled narrowband filters utilize coupling due to the even- and odd-mode velocity difference of coupled microstrip lines [10]–[12]. In order to eliminate all backward coupling, the resonator elements are coupled over their full half-wavelength extent, instead of the conventional quarter-wavelength.

Starting with the impedance matrix of two parallel coupled resonator sections with open ends, by using the pi-equivalent circuit as discussed in [21], we can obtain the short-circuit admittance. The resulting admittance inverter $J_{\rm ab}$ and resonator susceptance B_k are

$$J_{k,k+1} = J_{\rm ab} = \left| \frac{2[Z_{oe}Csc(\theta_e) - Z_{oo}Csc(\theta_o)]}{Z_{oe}^2 + Z_{oo}^2 - 2Z_{oe}Z_{oo}[Cot(\theta_e)Cot(\theta_o) + Csc(\theta_e)Csc(\theta_o)]} \right| \tag{6}$$

$$B_k = B_{k+1} = B = \frac{-2[Z_{oe}Cot(\theta_e) + Z_{oo}Cot(\theta_o)]}{Z_{oe}^2 + Z_{oo}^2 - 2Z_{oe}Z_{oo}[Cot(\theta_e)Cot(\theta_o) + Csc(\theta_e)Csc(\theta_o)]}. \tag{7}$$

The resonator slope parameter is then

$$b_k = b_{k+1} = \frac{\omega}{2}\frac{dB}{d\omega}\bigg|_{\omega=\omega_0} \tag{8}$$

and the coupling coefficient can finally be calculated as

$$k_{k,k+1} = \frac{J_{k,k+1}}{\sqrt{b_k b_{k+1}}} \tag{9}$$

where Z_{oe} and Z_{oo} are the even- and odd-mode impedances of the coupled lines, $\theta_e = \frac{\omega L}{c}\sqrt{\varepsilon_{er}^e}$ and $\theta_o = \frac{\omega L}{c}\sqrt{\varepsilon_{er}^o}$ are the electrical lengths corresponding to even- and odd-mode propagation, and ε_{er}^e and ε_{er}^o are the even- and odd-mode effective dielectric constants. The length of each resonator section can

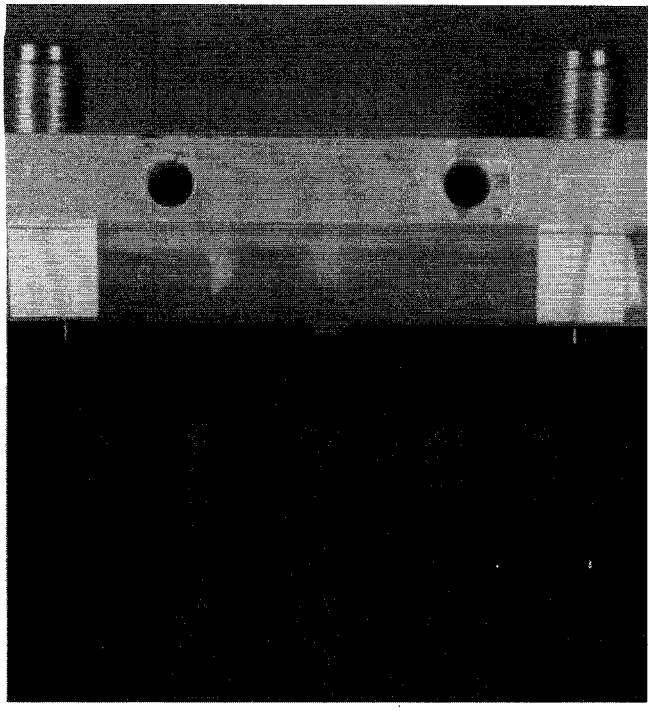

Fig. 5. A 5-pole, 2 GHz, 1.2% BW microstrip forward-coupled filter with 10-Ω line impedance on 508-μm-thick $LaAlO_3$ substrate. All five half-wavelength resonators are almost aligned.

be chosen such that $\frac{\theta_e+\theta_o}{2} = \pi$ for half-wavelength resonators. The spacing S between the adjacent resonators can be selected to achieve the proper coupling coefficient $k_{k,k+1}$ for a given design. Fig. 5 is a 5-pole forward-coupled filter centered at 2 GHz. It has 1.2% BW with 10-Ω resonator impedance on a 5-cm-diameter 508-μm-thick $LaAlO_3$ substrate.

III. Film Deposition and Filter Fabrication

In this work, we have used double-sided films made by off-axis sputtering using a noncontact gas-assisted substrate heater, magnetron sputtering [25] and coevaporation [26]. We also grow YBCO films on both sides of 5-cm-diameter $LaAlO_3$ substrates, using an off-axis laser ablation technique. The rotating substrates are heated by radiation using a cylindrical furnace, and films are deposited on both sides of the substrate simultaneously. Films for YBCO filters are also grown using MOCVD [27].

Processing of the high-power microstrip filters involves three steps: ground-plane contact layer deposition, patterning of the YBCO microstrip, and formation of ohmic contacts. We deposit a 0.5-μm gold film on the top of the YBCO on the ground plane side to improve the contact of the YBCO to the housing. The superconducting films are etched in a saturated aqueous solution of EDTA (ethylene diamine tetraacetic acid) purged with nitrogen. To obtain electrical contact on the input and output, a 0.5-μm silver contact pad is formed on the top of the YBCO using standard lift-off processing. Finally, the device is annealed at 450°C in oxygen. The filter is assembled in a gold-plated aluminum package, using a 127-μm-wide by 6-μm-thick gold ribbon, gap welded between the silver contact pads and the K-connector center pins.

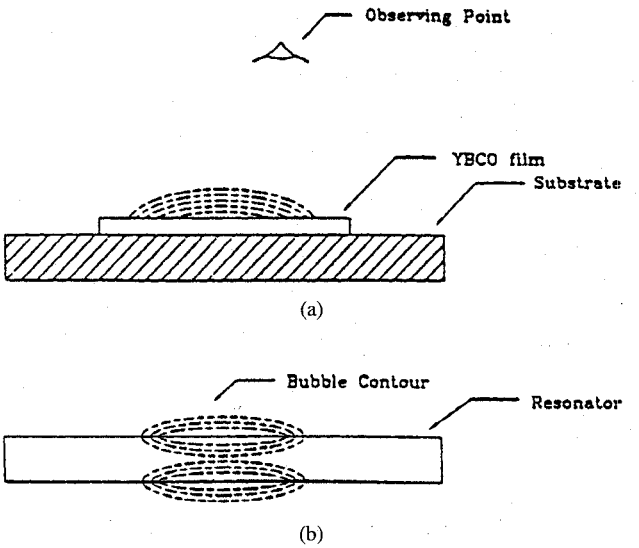

Fig. 6. Schematic diagram of helium bubbling on a YBCO thin-film filter resonator in an interdigital filter shown in Fig. 1. The rectangular area is the resonator and the contours correspond to the perimeter of the He boiling region at different power levels.

IV. Filter Performance

The low-power measurement is done with an HP8510 network analyzer with the filters under test submerged in liquid nitrogen (LN_2). The measurement of frequency response with different input powers at different temperatures is done in flowing helium gas. The TOI's are obtained by a standard two-tone intermodulation (IMD) measurement in which two single-frequency tones ω_1 and ω_2, of equal amplitude, are applied to the filter. Third-order mixing products, such as $2\omega_1 - \omega_2$, are observed in a spectrum analyzer at the output. The input power level of both tones is kept equal and varied simultaneously. In most cases, the third-order products are proportional to the cube of the input power and show a slope of 3 on a log-log plot, while the fundamental shows a slope of 1. The intersection of the slope 3 and slope 1 lines is the TOI and is the parameter normally used to characterize the IMD distortion. Knowledge of the TOI allows the calculation of the maximum operating power of the filter once the desired signal-to-spurious ratio is specified.

A. "Bubble" Imaging Technique

In order to understand the current distribution and heat dissipation distribution issues, we have developed a technique for imaging the spatial distribution of heat dissipation in filter structures by immersing the filter in liquid helium and observing the boiling pattern around the filter elements. This procedure is used to identify the current distribution in the geometric structures in a particular design. A camera is mounted outside the dewar to observe the boiling phenomena on the filter at different input powers. As the power passing through the filter increases, the current increases correspondingly. The surface resistance of the film results in increased dissipation with increasing currents. This dissipation initially leads to nucleate and, eventually, to film boiling of the helium bath. Fig. 6(a) shows the visualization of the bubbling. Fig. 6(b) is

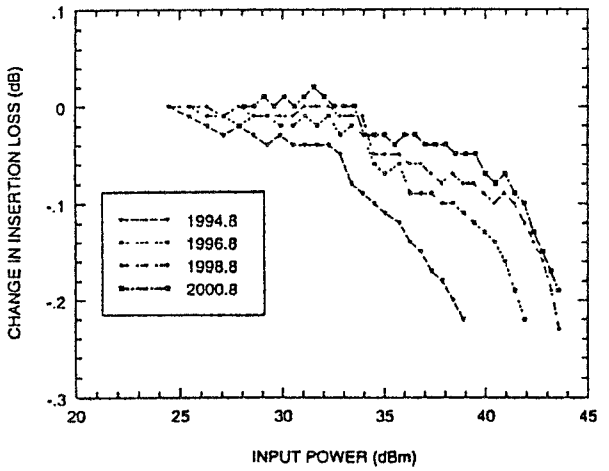

Fig. 7. Insertion loss increase versus input power of the forward- and backward-coupled filter shown in Fig. 4. Different curves represents different frequencies within the passband in MHz.

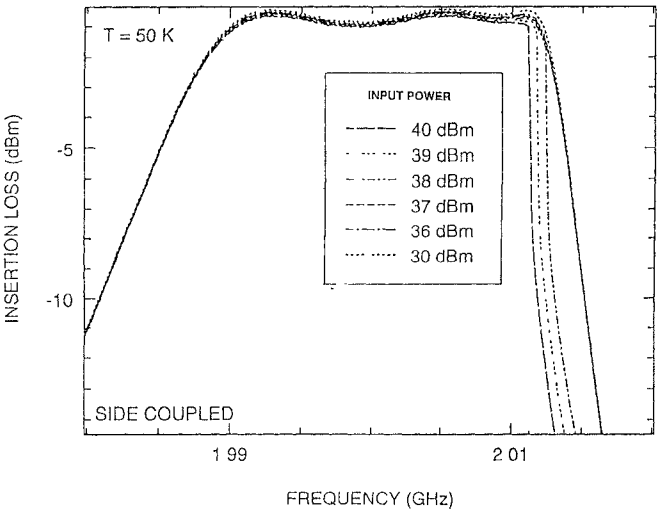

Fig. 8. Frequency response of the forward-coupled filter shown in Fig. 5 at 50 K with different input powers.

the view as seen by the camera through the transparent window of the dewar. The rectangular area is the resonator, and the contours correspond to the perimeter of the He boiling region at different power levels; the larger the enclosed area in the contour, the higher the power. From the location and intensity of the bubbling, we can identify the high dissipation areas. Also, by observing the bubbles at different operational conditions, we can identify how the current distribution changes with frequency in band, and how a plateau in dissipation in one area may lead to an onset of dissipation in another, indicating a redistribution of the currents.

B. Backward- and Forward-Coupled Filter Performance

Fig. 7 is the insertion loss variation of the filter shown in Fig. 4, as the input power is changed from a few mW to 25 watts (44 dBm). As can be seen, the relative change in insertion loss is less than 0.25 dB when the applied input power increases to 25 watts.

C. Forward-Coupled Filters Performance

Fig. 8 shows the measured filter response at different input power levels at 50 K for the forward-coupled filter shown in Fig. 5. The wafer was bonded to a thermally matched package and was tested in a cryocooler. The dissipation loss (minimum loss cross the band) at 45 K was less than 0.25 dB and the return loss was better than 12 dB. We applied 10 watts to the filter at 50 K with 0.1 dB compression. At 35 K, it takes over 20 watts of CW. Fig. 9 shows the intermodulation measurement of this filter at 45 K. The TOI is 62 dBm with best linear fit. The upper curve is the fundamental mode output per tone, and the lower curve is the third-order output. All measured power are per tone. In the measurement, the inputs are at 2000 $\pm$ 0.5 MHz.

The nonlinear behavior of the filter is due to the film's nonlinear response. For an ideal transmission line with a characteristic impedance of Z_0, the voltage-current relationship of a traveling wave is governed by $Z(t) = I(t)Z_0$, and the

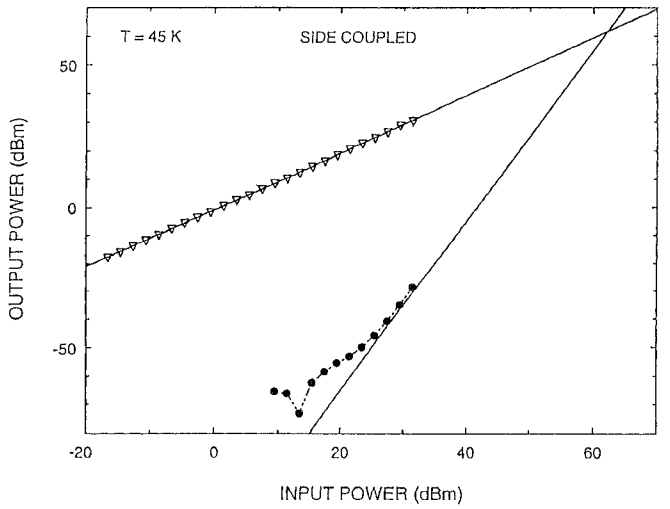

Fig. 9. Intermodulation measurement of the filter shown in Fig. 5 at 45 K. The TOI is 62 dBm with best linear fit. The upper curve is the fundamental mode output per tone, and the lower curve is the third-order output with inputs at 2000 $\pm$ 0.5 MHz. All measured powers are per tone.

voltage has the same frequency components as the current. For a transmission line with nonlinear surface impedance, $Z = Z(I)$, the voltage will be a nonlinear function of current, $V(t) = I(t)Z(I) = a_1 I(t) + a_2 I^2(t) + a_3 I^3(t) + \cdots$. If we apply a two tone signal $I(t) = I_1 \cos \omega_1 t + I_2 \cos \omega_2 t$, it will produce harmonics at frequencies $m\omega_1 \pm n\omega_2$ where m and n are integers. Among these high order terms, the 3rd-order IMD signals $2\omega_1 - \omega_2$, $2\omega_2 - \omega_1$ are nearly the same frequency as ω_1 or ω_2 if ω_1, ω_2 are very close to each other. These signals, therefore, may fall in the bandwidth of the filter and hence are the most troublesome terms, limiting the linear dynamic and spur-free dynamic range. Although the phenomenon is not completely understood, it has been suggested that the cause of power dependence of the superconducting film is Josephson-junction like defects due to the grain boundaries. Since the films are not homogeneous, the weak link junctions

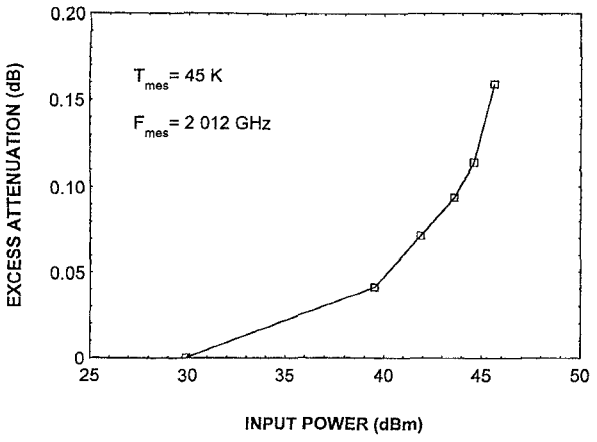

Fig. 10. Insertion loss of the forward-coupled filter in Fig. 5 at 45 K with the increase of the input power at the upper band edge (at 2.012 GHz).

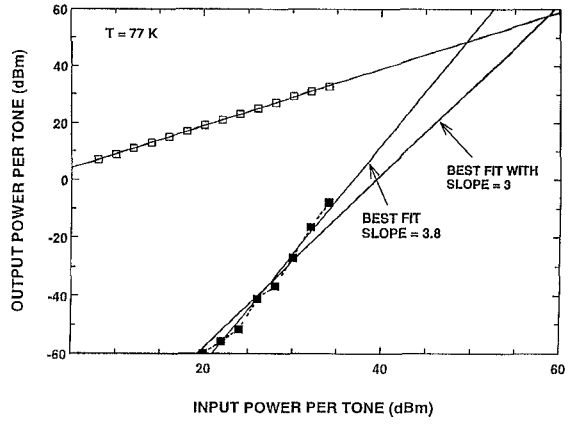

Fig. 11. Intermodulation measurement of the forward-coupled filter shown in Fig. 5 at 77 K. The TOI is 49 dBm with best linear fit and is 57 dBm with best fit of curve with a slope of 3. The inputs are at 2000 ± 0.5 MHz. Both horizontal and vertical axes are power per tone. The TOI at lower temperature is much higher.

have different critical currents, resulting in the change of the 3rd-order output slope [28]–[30].

The second purely forward-coupled filter as shown in Fig. 5 handled 36 watts of power at 45 K with a maximum compression of 0.15 dB at the upper band edge, Fig. 10 shows the relative insertion loss changes with respect to the input power, as the input power was changed from a few mW to 36 watts (45.6 dBm). Fig. 11 shows the third-order intercept at 77 K and with the linear curve fit (with a slope of 3) and a linear best fit of arbitrary slope (3.8). The TOI of the filter for two different fitting schemes are 57 dBm and 49 dBm.

V. Conclusion

We have discussed the design, fabrication, and testing of high-power HTS filters. Design techniques for maximizing the power-handling capabilities of these filters, such as the use of low-impedance resonators, were presented. We reported two types of filters with low internal characteristic impedances. One mixed backward- and forward- coupled has handled over 25 watts at 10 K. Another type of filter reported is a forward-coupled filter, one of them has 1.2% BW and 10-Ω resonator internal impedance and handled more than 10 watts of power at 50 K. Second purely forward-coupled filter handled 36 watts of power at 45 K, with a maximum band edge compression of 0.15 dB as the applied input power increases to 36 watts.

Acknowledgment

The authors would like to thank L. L.-Wong and A. Barfknecht at Conductus, R. Slattery and R. Konieczka at MIT Lincoln Laboratory, and P. Kerney and B. Andeen at CTI-Cryogenics for their valuable assistance. They would also like to thank J. Rowell at Conductus and R. Ralston at Lincoln Laboratory for encouragement of this work.

References

[1] M. Paetsch, *Mobile Communications in the US and Europe: Regulation, Technology, and Market*. Boston: Artech House, 1993.
[2] W. C. Y. Lee, *Mobile Cellular Telecommunications Systems*. New York: McGraw-Hill, 1989.
[3] N. J. Boucher, *The Cellular Radio Handbook*, 3rd ed. Mill Valley CA: Quantum Publishing, 1995.
[4] W. G. Lyons, R. S. Withers, J. M. Hamm, A. C. Anderson, P. M. Mankiewich, M. L. O'Malley, R. E. Howard, R. R. Bonetti, A. E. Williams, and N. Newman, "High-temperature superconductive passive microwave devices," in *1991 IEEE Int. Microwave Symp. Dig.*, Boston, MA, June 1991, pp. 1227–1230.
[5] M. S. Schmidt, R. J. Forse, R. B. Hammond, M. M. Eddy, and W. L. Olson, "Measured performance at 77 K of superconducting microstrip resonators and filters," *IEEE Trans. Microwave Theory Tech.*, vol. 39, pp. 1475–1479, Sept. 1991.
[6] A. Fathy, D. Kalokitis, V. P. Pendrick, E. Belohoubek, A. Pique, and M. Mathur, "Superconducting narrowband pass filters for advanced multiplexers," in *1993 IEEE Int. Microwave Symp. Dig.*, Atlanta, GA, June 1993, pp. 1277–1280.
[7] G. L. Matthaei and G. L. Hey-Shipton, "Novel staggered resonator array superconducting 2.3-GHz bandpass filter," in *1993 Int. IEEE Microwave Symp. Dig*, Atlanta, GA, June 1993, pp. 1269–1272.
[8] ——, "High temperature superconducting 8.45-GHz bandpass filter for the deep space network," *1993 Int. IEEE Microwave Symp. Dig.*, Atlanta, GA, June 1993, pp. 1273–1276.
[9] D. E. Oates, W. G. Lyons, and A. C. Anderson, "Superconducting thin-film $YBa_2Cu_3O_{7-\delta}$ resonator and filters," *Proc. Forty-Fifth Annual Sym. on Freq. Contr.*, 1991, pp. 460–466.
[10] G. C. Liang, D. Zhang, C. F. Shih, R. S. Withers, M. E. Johansson, W. Ruby, B. F. Cole, M. Krivoruchko, and D. E. Oates, "High power HTS microstrip filters for wireless communication," *1994 Int. IEEE Microwave Symp. Dig.*, San Diego, CA, May 1994, pp. 183–186.
[11] D. Zhang, G.-C. Liang, C. F. Shih, R. S. Withers, M. E. Johansson, and A. Dela Cruz, "Compact forward-coupled high-temperature superconducting filters for cellular communications," in *1994 Applied Superconductivity Conf.*, Boston, MA, Oct. 1994, pp. 2656–2659.
[12] D. Zhang, G.-C. Liang, C. F. Shih, M. E. Johansson, and R. S. Withers, "Accurate design of compact forward-coupled microstrip filters using an integral-equation field solver," *Int. J. Computer Aided Design*, vol. 5, no. 5, pp. 324–330, 1995.
[13] J. X. Zheng, "A general purpose 3D electromagnetic simulation and optimization package-IE 3D," in *1994 Int. Microwave Symp. Dig.*, San Diego, CA, May 1994, pp. 373–376.
[14] G. C. Liang, Y. W. Liu, and K. K. Mei, "Propagation properties of a superconductive stripline," in *1990 Int. IEEE Antenna Propagation Symp. Dig.*, Dallas, TX, May 1990, pp. 728–731.
[15] R. Pous, G. C. Liang, and K. K. Mei, "Modeling of superconductivity for EM boundary problems," *Directions in Electromagnetic Waves Modeling*. New York: Plenum, 1990, pp. 467–476.
[16] G. C. Liang, "High-temperature superconductor microwave circuits," Ph.D. Dissertation, Dept. of Electrical Engineering and Computer Science, Univ. of California, Berkeley, Nov. 1990.
[17] J. Halbritter, "On intrinsic and extrinsic effects in the surface impedance of Cuprate superconductors," *J. Superconductivity*, vol. 5, pp. 331–337, Aug.1992.

[18] J. R. Clem and M. W. Coffey, "Effects of flux flow, flux pinning and flux creep upon the rf surface impedance of type-II superconductors," *J. Superconductivity*, vol. 5, pp. 313–318, Aug. 1992.
[19] P. P. Nguyen, D. E. Oates, G. Dresselhaus, and M. S. Dresselhaus, "Nonlinear surface impedance for $YBa_2Cu_3O_{7-\delta}$ thin film: Measurements and a coupled-grain model," *Phys. Rev B*, vol. 48, pp. 6400–6412, Sept. 1993.
[20] D. M. Sheen, S. M. Ali, D. E. Oates, R. S. Withers, and J. A. Kong, "Current distribution, resistance and inductance for superconducting strip transmission lines," *IEEE Trans. Appl. Superconduct.*, vol. 1. pp. 108–115, June 1991.
[21] G. L. Matthaei, L. Young, and E. M. T. Jones, *Microwave Filters, Impedance-Matching Network, and Coupling Structures*. Dedham, MA: Artech House, 1980.
[22] C. W. Lam, D. M. Sheen, S. M. Ali, and D. E. Oates, "Modeling the nonlinearity of superconducting strip transmission lines," *IEEE Trans. Appl. Superconduct.*, vol. 2, pp. 58–66, June 1992.
[23] G. C. Liang, D. Zhang, C.-F. Shih, M. E. Johansson, R. S. Withers, A. C. Anderson, and D. E. Oates, "High-power high-temperature superconducting microstrip filters for cellular applications," in *1994 Applied Superconductivity Conf.*, Boston, MA, Oct. 1994.
[24] G.-C. Liang, D. Zhang, C.-F. Shih, M. E. Johansson, R. Withers, A. C. Anderson, D. E. Oates, P. Polakos, P. Mankiewich, E. de Obaldia, and R. E. Miller, "High-temperature superconducting microstrip filters with high power-handling capability," *IEEE Int. Microwave Symp.*, Orlando, FL, May 15–19, 1995.
[25] A. C. Anderson and R. L. Slattery, "YBCO thin films for microwave applications," in *1994 Applied Superconductivity Conf.*, Boston, MA, Oct. 1994.
[26] H. Kinder, P. Berberich, B. Utz, and Prusseit, "Double sided YBCO films on 4" substrates by thermal reactive evaporation," in *1994 Appl. Superconductivity Conf.*, Boston, MA, Oct. 1994.
[27] Z. Lu, J. K. Truman, M. E. Johansson, D. Zhang, C. F. Shih, and G. C. Liang, "Large area double-sided YBCO films grown by single-source MOCVD," *Appl. Phys. Lett.*, vol. 67, pp. 712–714, July 1995.
[28] J. H. Oates, R. T. Shin, D. E. Oates, M. J. Tsuk, and P. P. Nguyen, "A nonlinear transmission line model for superconducting stripline resonator," *IEEE Trans. Appl. Superconduct.*, vol. 3, pp. 17–21, Mar. 1993.
[29] A. M. Portis, "Microwave power-induced flux penetration and loss in high-temperature superconductors," *J. Superconductivity*, vol. 5, pp. 319–330, Aug. 1992.
[30] N. Newman and W. G. Lyons, "High-temperature superconducting microwave devices: Fundamental issues in materials, physics, and engineering," *J. Superconduct.*, vol. 6, pp. 119–160, 1993.

Guo-Chun Liang (S'87-M'90–SM'94) received the B.S. degree from the East China Institute of Technology, Naijing, China, in 1982, the M.S. degree from the University of Electronics Science and Technology of China (UEST), Chengdu, China, 1985, and the Ph.D. degree from University of California at Berkeley, in 1990, all in electrical engineering.

He worked at the microwave center of UEST in 1985 to 1986. He developed a series of RF and microwave devices, including low noise amplifiers, high power amplifiers, cellular phone package and antenna, attenuators, oscillators, phase shifters, and filters. He also has done a variety of time-domain numerical analyses and simulations of rf and microwave devices such as transmission lines, amplifiers, antennas, and semiconductor and superconductor devices. He has been with Conductus, Inc. since 1990, developing superconductive rf and microwave circuits and systems, including resonators, filters, mixers, delay lines, and magnetic resonance coils. He led the development of space-qualified instantaneous frequency-measurements system for the Navy's High-Temperature Superconductor Space Experiment program (II). He is coordinating Conductus's effort in Consortium for Superconducting Electronics activities, collaborating with MIT Lincoln Laboratory, AT&T and CTI on high-temperature superconductor wireless product. Currently, he is a manager in wireless technology leading the development of superconductive circuits and subsystems and cryogenically cooled electronics for wireless communication applications. His interests include rf and microwave applications of superconductivity, microwave circuits and systems, cellular phone applications, numerical analysis and simulation of practical electromagnetic problems.

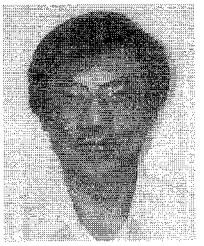

Dawei Zhang (M'93) received the B.S. degree in physics from the University of Science and Technology and China in 1987, and the M.S. and Ph.D. degrees in physics from the University of California at Los Angeles, in 1988 and 1992, respectively.

From May 1992 to May 1994, he was a postdoctoral fellow with the Consortium for Superconducting Electronics, working on the development of a millimeter-wave confocal resonator in applications in surface resistance scanning, semiconductor vertical doping profile determination, and dielectric constant and loss tangent mapping. Prior to that in his graduate study at UCLA, he developed 92 GHz quasioptical millimeter-wave frequency-selective surfaces using high-temperature superconducting thin films. He has been with Conductus, Inc. since May 1994 as a member of the technical staff, where as an RF circuit designer, he developed various planar circuit structures suitable for applications of the high-temperature superconductors in cellular filter application, including microstrip forward-coupled filter structure, thin film lumped-element filters, and microstrip narrow-band filter structure using a novel frequency-transformation technique. Currently he is working on the designing and development of superconducting circuits and subsystems and cryogenically cooled RF and microwave electronics for wireless communication applications. His interests are in the microwave and RF applications in such field as communications and RF instrumentation.

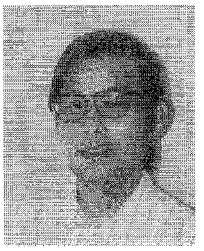

Chien-Fu Shih received B.S. degree in physics from Fu-Jen University, Taiwan, in 1969, the M.S. degree in physics from University of Winconsin, Superior, in 1972, and the M.S.E.E. degree from Oregon State University, Corvalis, in 1978.

From 1978 to 1981, he was with Eaton Corporation as a Microwave Engineer developing voltage controlled oscillators and multipliers. Later, he worked as an integration Engineer at Ford Aerospace Corporation, designing the transponder circuits. In 1984, he joined Hewlett Packard Company as an Electrical Engineer designing at Tracking Generator. In 1992, he joined Conductus, Inc. Since then he has been involved in the design and measurement of superconductive microwave subsystems, resonators, and filters.

Marie E. Johansson received the B.S. degree in physics from the University of Linkoeping, Sweden, 1986.

From 1986 to 1989, she designed and produced passive microwave devices at the National Defense Research Institute in Linkoeping, Sweden. She then developed process techniques for high-T_c thin films at the National Institute of Standards the Technology, Boulder, CO. Since joining Conductus in June 1992, she has been working on the development and processing of high-T_c superconducting microwave and digital devices.

Richard S. Withers (M'78) received the S.B. and S.M. degrees in 1976, and the Sc.D. degree in 1978, all in electrical engineering, from the Massachusetts Institute of Technology.

He joined Conductus, where he is the Manager of Magnetic Resonance and RF Technology, in July 1991 from the M.I.T. Lincoln Laboratory, where he was Associate Leader of the Analog Device Technology Group. In that capacity he co-directed Lincoln's development of microwave circuits using high-temperature superconductors. Previously, as a member of the technical staff at Lincoln from 1978 to 1984, he developed niobium tapped delay lines, silicon charge-coupled devices, and surface-acoustic-wave devices. Withers was the program manager for microwave networks within the Consortium for Superconducting Electronics until October 1992, and in that capacity coordinated efforts at Conductus, Lincoln Laboratory, IBM, AT&T Bell Laboratory, M.I.T., Cornell University, and Boston University. His interests are in the microwave and RF applications of superconductivity in such fields as communications, RF instrumentation, and magnetic-resonance instruments.

Dr. Withers is active in the microwave and RF superconductivity community. He served on the advisory panel of the High-Temperature Superconductivity Assessment of the Office of Technology Assessment of the US Congress and briefed the Defense Science Board Task Force on Military System Applications of Superconductors. He has given short courses on RF applications of superconductivity for audiences at the Nordic Symposium on Superconductivity and the 1991 SPIE Conference on superconductive electronics. He co-chaired, with Robert B. Hammond, the SPIE Conference on High-T_c Microwave Superconductors and Applications in Jan. 1994.

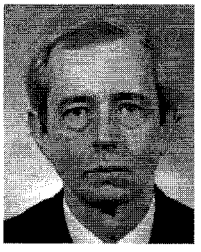

Daniel E. Oates received the B.A. degree in physics from Yale University in 1965 and the Ph.D. degree in physics from the Massachusetts Institute of Technology in 1971.

From 1973 to 1978 he was with Bell Laboratories, Holmdel, NJ. Since 1978 he has been at Lincoln Laboratory. His research at Lincoln Laboratory has included investigations of surface acoustic wave and bulk wave devices. Since 1988 his primary research interests have been in superconducting electronic, especially applications in frequency control and microwave-frequency analog signal processing. Motivated by the applications of superconductors, he has investigated the fundamental properties of superconductors at microwave frequencies and at high microwave power levels.

Dr. Oates held an Alexander von Humboldt fellowship at the University of Bonn, Federal Republic of Germany in 1971–72.

A. C. Anderson, photograph and biography not available at the time of publication.

P. Polakos, photograph and biography not available at the time of publication.

P. Mankiewich, photograph and biography not available at the time of publication.

E. de Obaldia, photograph and biography not available at the time of publication.

R. E. Miller, photograph and biography not available at the time of publication.